Precise control of thermal conductivity at the nanoscale through individual phonon-scattering barriers

Gilles Pernot, M. Stoffel, I. Savic, F. Pezzoli, P. Chen, Guillaume Savelli, A. Jacquot, J. Schumann, U. Denker, I. Mönch, et al.

To cite this version:

Gilles Pernot, M. Stoffel, I. Savic, F. Pezzoli, P. Chen, et al.. Precise control of thermal conductivity at the nanoscale through individual phonon-scattering barriers. Nature Materials, 2010, 9 (6), pp.491-495. 10.1038/NMAT2752 . hal-00505811

Precise control of thermal conductivity at the nanoscale via individual phonon scattering barriers

G. Pernot[1], M. Stoffel[2], I. Savic[3], F. Pezzoli[2], P. Chen[2], G. Savelli[3], A. Jacquot[4], J. Schumann[2], U. Denker[5], I. Mönch[2], Ch. Deneke[2], O.G. Schmidt[2], J. M. Rampnoux[1], S. Wang[3], M. Plissonnier[3], A. Rastelli[2,]*, S. Dilhaire[1,]*, and N. Mingo[3,]*

[1]CPMOH, Université Bordeaux-CNRS, 351 cours de la Libération 33405 Talence, France.

[2]Institute for Integrative Nanosciences, IFW Dresden, Helmholtzstr. 20, 01069 Dresden, Germany.

[3]LITEN, CEA-Grenoble, 17 rue des Martyrs, Grenoble 38000, France.

[4]Fraunhofer-IPM, Heidenhostraße 8, 79110 Freiburg, Germany.

[5]Max-Planck-Institut für Festkörperforschung, Heisenbergstr. 1, 70569 Stuttgart, Germany.

* Corresponding authors, stefan.dilhaire@u-bordeaux1.fr, a.rastelli@ifw-dresden.de, natalio.mingo@cea.fr

The ability to precisely control the thermal conductivity (κ) of a material is fundamental in the development of on-chip heat management or energy conversion applications. Nanostructuring permits to dramatically reduce κ of single-crystalline materials, as recently demonstrated for silicon nanowires. However, silicon-based nanostructured materials with extremely low κ are not limited to nanowires. By engineering a set of individual phonon scattering nanodot barriers we have accurately tailored the thermal conductivity of a single-crystalline SiGe material in spatially defined regions as short as ~15 nm. Single barrier thermal resistances between 2-4×10^{-9} m^2 K/W were attained, resulting in a room temperature κ down to about 0.9 W/m-K, in multilayered structures with as little as 5 barriers. Such low thermal conductivity is compatible with a totally diffuse mismatch model for the barriers, and it is well below the amorphous limit. The results are in agreement with atomistic Green's function simulations.

Accurately tailoring the thermal conductivity of nanostructured materials with high spatial resolution is a fundamental challenge for micro and nanoelectronics heat management, and for micro/nano scale energy conversion on a chip [1-4]. Previous work on nanoscale thermal transport has demonstrated that in some cases nanostructuring can reduce the thermal conductivity of a material below that of its disordered alloy counterpart [5-7], and can even beat the amorphous limit [8], which for a long time was believed to represent a bound to the minimum attainable thermal conductivity of a material with a given composition [9]. In dislocation-free SiGe/Si multilayered materials however, it has not been clear how low the thermal conductivity can be pushed. A plausible lower bound when the SiGe layers are very thin would be given by a model in which ballistic Si layers are separated by interfaces, or phonon barriers (the thin SiGe regions), where phonons are scattered in a completely diffusive way. This is the diffuse mismatch model, DMM, in the particular case of no acoustic mismatch between the two sides of the interface [10]. In general, however, previous works only showed a weakly diffusive behavior of the interfaces, with layer resistances lower than those predicted by the diffuse mismatch model. When the layers are composed of nanodots, this may be due to the low areal fraction covered by the interface dots [7]. However, in the opposite limit of fully continuous SiGe interlayers, the room temperature interface thermal resistance is also about 3 times lower than the DMM [6]. This raises the question: is it possible to achieve highly diffusive interfaces in SiGe/Si systems? Besides, most previous measurements were performed on systems above 1 μm thick and comprising over a hundred periods. Thus, it was unclear whether much thinner systems would still preserve the individually additive character of the single interface resistance, or whether ballistic effects across multiple periods might occur, rendering the concept of thermal conductivity inadequate for such thin regions [11].

Here we answer the two questions above, and show that: (1) highly diffusive interfaces can be achieved in dislocation-free SiGe/Si nanodot systems; and because of this, (2) a well defined thermal conductivity can be accurately tailored for material regions as short as ~15 nm, comprising just a small number of periods. Two independent measurement techniques (see “methods” and “supplementary material”), Heterodyne Picosecond Thermoreflectance (HPTR) and the differential 3ω method, were employed to evaluate the thermal conductivities, yielding results consistent with an atomistic Green’s function simulation of the phonon transport through the SiGe nanodot barriers.

The structures studied here (see sketch in Fig. 1a) consist of 5 and 11 layers of epitaxial Ge nanodots separated by Si spacers with thickness t_{Si} (see “methods”). The first island layer was obtained by deposition of about 6 monolayers (ML) Ge leading to the formation of small {105} faceted islands on top of a 3-4 ML thick wetting layer (Fig. 1c). Dots have an average height of 1.2±0.2 nm and a surface density of $\sim 8 \cdot 10^{10}$ cm^{-2}, with a fractional area coverage of about 70%. In the upper layers, the Ge coverage was reduced in order to prevent the occurrence of misfit dislocations [12], as verified by extensive transmission electron microscopy (TEM) investigations (see, e.g., Fig. 1b). In comparison with most of the previous works [7,13,14], our multilayers were grown at lower substrate temperature (500°C), resulting in smaller dots (“hut-” instead of “dome-” and “pyramid-” shaped clusters) with higher Ge content and higher surface densities. From atomic force microscopy (AFM) measurements performed on the topmost layer of the stack (see Fig. 1d) we find that the areal densities in different samples vary between 1.2 to $5 \cdot 10^{10}$ cm^{-2}, which is significantly larger than those explored so far (up to $\sim 7 \cdot 10^{9}$ cm^{-2} in [7]). Only in Ref. [15] the same nominal growth temperature was used, but the study was limited to relatively large interlayer spacing (20 nm) and low density islands ($7 \cdot 10^{9}$ cm^{-2}).

In order to characterize the cross-plane thermal conductivity, κ, of the samples we have developed the HPTR approach [16]. Numerous authors mentioned [17-21] that the standard homodyne configuration of the Picosecond Thermoreflectance technique introduces a number of artifacts in the experimental signal and need to undergo a number of corrections before a correct interpretation of the signal can be carried out. The most important artifacts are: residual pump signal on the photodetector, misalignment of the pump and the probe beams, and spot size change as a function of the delay line position. All these artifacts induce systematic errors in the identification procedures used to extract thermal and acoustic material properties [22-24]; they are inherent to this kind of configurations and affect the uncertainty on the identified thermal properties. To fix all these sources of artifacts, we eliminated any mechanical translation stage and modulation using two heterodyne pump and probe laser beams at slightly different repetition rates. Then there was no need for the lock-in amplifier and the signal was acquired by using only an oscilloscope. (See methods.)

HPTR measurements were carried out at the University of Bordeaux on the samples with 5 and 11 Ge layers, and independent 3ω measurements were carried out at IFW Dresden on samples with 11 Ge layers, yielding results consistent with those from HPTR. The results are shown in Fig. 2, where the cross-plane thermal resistance per interface R (Fig. 2a) and the thermal conductivity of all the samples (Fig. 2b) are plotted as a function of multilayer period thickness L. (L is estimated as the sum of t_{Si} and the average amount of Ge per dot layer t_{Ge}). The quoted error bars take into account different sources of uncertainties: for the 3ω measurements they represent confidence intervals (at 68% confidence level) estimated by propagating the uncertainties in the experimental parameters (metal strip widths, electric power etc.) via the Monte Carlo method; for the HPTR … (for details see “Supplementary Material”). It was previously shown that the 3ω and thermoreflectance measurements compare well with each other [25], as confirmed by the excellent agreement between the results obtained on the samples with 11 Ge layers. The differences between the results obtained on the two different sample sets by HPTR may be ascribed to the slightly different amounts of Ge used in the growth of the two sample sets.

It is illuminating to normalize the thermal resistance values of Fig. 2a by the average amount of Ge contained in each interface, given in terms of its thickness t_{Ge}. When this is done, one obtains a nearly constant thermal resistivity, of about 4.5 m K W^{-1} for a single layer, independent on the period (Fig. 2c). This strongly suggests that transport through the Si regions is ballistic, and resistance is produced by the independent nanodot layers: each layer acts as an individual barrier, and the total thermal resistance is the sum of the individual barrier resistances. Such a picture is consistent with the fact that the average phonon mean free path in Si is larger than a hundred nm [42]. The phonon mean free path is thus determined by scattering with the SiGe nanodots, which are arranged in individual layers, perpendicular to the direction of heat propagation, and separated by a distance L between each consecutive layer. In an overly simplistic view, a fully diffusive barrier will have equal transmission and reflection probabilities of ½, yielding the limit $\lambda \sim L$ for the mean free path. The thermal conductivity can now be evaluated as an integral over frequencies [26], obtaining the DMM limit shown by the solid line in Fig. 2b. The measured thermal resistance associated to one individual interface is around $2.5\text{-}4 \cdot 10^{-9}$ m^2K/W. This is close to the DMM value in the totally diffuse case (see Fig. 2b), and it is 2-3 times larger than the values reported in Refs. [6, 7].

The above implies that a very precise control over the thermal conductivity value of the nanostructured material can be achieved by varying the period length. As a result of the highly diffusive character of the interfaces, we are able to reach the very low thermal conductivity value of (0.9±0.1) W/m-K when using periods of ~3.7 nm (5 nanodot layers separated by 4 Si spacings, with a total thickness of 15.5 nm and an average barrier resistance of $3.5 \cdot 10^{-9}$ m^2K/W in this case). This thermal conductivity is the lowest reported so far for bulk-like Si or SiGe samples, and it is well below the amorphous Si limit of 2.5 W/m-K [27]. A smaller thermal conductivity of 0.76 W/m-K was reported only for 10-nm-wide Si nanowires [28,29]. A value of 1.2 W/m-K was independently reported on rough Si nanowires [29,30].

To rule out the presence of extended defects, we have carried out AFM investigations on large areas of the samples in addition to TEM. It is in fact known that the occurrence of dislocations during the fabrication of the multilayer will locally disrupt the growth of Si or Ge leading to the formation of either large Ge islands or pits/mounds in the Si cap layer. For the samples with smallest period and smallest cross-plane thermal conductivity (t_{Si} = 3 and 6 nm) we were not able to detect any such features in an area as large as $60 \cdot 60\ \mu m^2$ (see Supplementary Material). Thus we can consider the system as dislocation free, and the low measured thermal conductivities are the result of phonon scattering by the nanostructures alone.

The additive character of the individual interface thermal resistances allows us to engineer regions with accurately defined values of κ, with good spatial resolution down to the 10 nm level. In our samples, the shortest measured region was ~15 nm thick, consisting of 5 interfaces. Previous publications have shown that the thermal conductivity may display a minimum as a function of period length if the periods are reduced below 4 nm (for $BiSbTe_3$ superlattices) or 7 nm (for SiGe superlattices) [31-33]. However, we did not observe any such minimum down to the ~3.7 nm period size. Since such "thermal conductivity minimum" is related to the onset of wave interference effects across the interfaces, its absence from our results reinforces the conclusion that scattering at the nanodot layers is highly diffusive.

It is intriguing that previous measurements on “flat” SiGe/Si superlattices had reported thermal conductivity values about 3 times larger than our results and the DMM at room temperature. To elucidate the reasons for this difference, we have performed an atomistic Green’s function (AGF) calculation (see “methods”) of the thermal conductivities of both a flat multilayer, and a quantum dot multilayer system, comprising 4 barriers (Fig. 2d.) We first computed the thermal conductivity of a bulk $Si_{0.5}Ge_{0.5}$ alloy, obtaining a value of 14.5 W/m-K, of similar order of magnitude as the experimental one [34]. We have then computed the thermal conductivity of 4 “flat” $Si_{0.5}Ge_{0.5}$ barriers 1.63 nm thick, placed into pure Si, with periods of 3.26, 6.52, 9.78 and 13.04 nm (triangles in Fig. 2d.) Finally, the thermal conductivity of nanodot superlattices with the same period lengths has been computed, obtaining results (diamonds in Fig. 2d) close to the DMM and in reasonably good agreement with our experimentally measured ones. Due to the approximations used, and to inaccuracies in the phonon dispersion description given by the Tersoff potential used (see methods), we do not expect a perfect agreement between theoretical and experimental results. Similarly as in the experiment, the AGF calculation yields a rather linear dependence of thermal conductivity with period length. We have also performed calculations with 10 layers, which yield nearly the same results. The AGF thermal conductivity results for the flat barriers are considerably larger than the ones with the additional effect of the nanodots (diamonds in Fig. 2d). A closer look at the flat superlattice MFPs (see “supplementary materials”) shows that at low frequency they are considerably longer than those for the nanodot multilayer, but the two are comparable at high frequency. This is because the roughness, or interface disorder, of the flat superlattices lacks the larger feature sizes introduced by the dots, whereas at short wavelengths the two systems look quite similar. Our flat superlattice theoretical results are of the same order as the measurements in Ref. [6]. Thus, this suggests that the lack of larger size roughness features was the reason for the larger thermal conductivities reported there, as compared to our measurements.

The results presented are also striking because they show that a very low thermal conductivity can be achieved using a pure Si matrix. It has been theoretically shown that Si matrix nanodot composites may be expected to display a much larger thermal conductivity than SiGe matrix nanodot composites, due to the different frequency dependence of the phonon mean free path in the two types of matrix [35]. Our samples however achieve κ below both the alloy and the amorphous limit with a total Ge volume fraction below 20%. Since the dots in our sample are very flat and arranged in layers, contrasting with the disordered spherical dots of Ref. [35], a direct comparison is not possible. However, we speculate that similar measurements performed on samples of pure Ge nanodots embedded into a SiGe matrix might yield thermal conductivity values even lower than the ones reported here.

This demonstrated ability to tailor thermal conductivity with 1W/m-K precision and a spatial resolution below the 20 nm range is very relevant to the development of integrated miniaturized energy harvesting or thermal management devices, fully compatible with silicon nanoelectronics. The highly diffusive interfaces achieved permit the precise control of thermal conductivity at the local level, via the sole distance between interfaces. A similar approach could be used with other materials, thus extending the range of thermal conductivities available, and possibly being able to simultaneously tailor electronic properties as well.

Methods:

Sample growth and structural characterization

All samples were grown by solid source molecular beam epitaxy (MBE) on Si(001) substrates and consist of multilayers of coherently strained Ge/Si islands (or nanodots) obtained with the Stranski-Krastanow growth mode. The substrate temperature was 500°C both during island growth and Si capping. A reference samples containing only a Si layer grown under the same conditions was fabricated for measurements with the 3ω method. We used AFM in tapping mode to characterize the nanodot properties (size/density) and large-area AFM and TEM to detect signatures of extended crystal defects. Further details on growth parameters and structural characterization are included in the Supplementary Material.

Heterodyne Picosecond Thermoreflectance (HPTR)

Figure 3 illustrates the schematic diagram of the experimental set-up for heterodyne configuration of the Picosecond Thermoreflectance. Two femtosecond oscillators are used as pump and probe beams. Their repetition periods (τ_P and τ_S) are slightly different and the two beams are focused on the sample with a microscope objective; their wavelengths can be adjusted independently. The probe beam is detected with a photodiode and the signal *S(t)* is recorded by a digital oscilloscope. A beam splitter deviates a part of the two reflected beam to a photodiode in order to obtain a synchronization signal.

$$S(t) \propto \sum_{p=-\infty}^{+\infty} \Delta T\left(t - p\cdot\tau_P\right) \sum_{n=-\infty}^{+\infty} \delta\left(t - n\cdot\tau_S\right)$$

ΔT is the surface temperature variation induced by a single pump pulse. The sum over *p* is the convolution between the pump pulse train and the impulse temperature response of the material, while the sum over *n* is the probe pulse train sampling the response.

Thermal properties identification

A Levenberg-Marquardt minimization algorithm coupled to a 3D thermal model with cylindrical symmetry has been developed for a multilayer structure. The thermal properties are extracted through the optimization of the fitting of the experimental signal to the theoretical thermal model. In most cases the sample studied consists of an active layer in between the top metal transducer film and the substrate. Thermal properties accessible with HPTR, thanks to the 12,5 ns time range, are the cross-plane thermal conductivity of the active layer and the Kapitza resistances of each interface. The absence of any mechanical artifacts permits to achieve a reliable identification of the value of each thermal property. The uncertainty is only depending on the knowledge of the fixed parameters. Most of them were measured with other experimental approaches (AFM or profilometry for metal thicknesses) while specific heat was taken from literature.

Differential 3ω method

Thin metal strips (about 7 μm wide), acting both as electrical heaters and thermometers, were placed on the surface of the multilayer samples and on a reference sample [27]. Thin (30 nm-thick) Al_2O_3 layers grown by atomic layer deposition were employed as electric insulators between strips and samples because of their relatively high thermal conductance. At a given heating power, the temperature rise measured on the metal strip is a function of the underlying material properties（density, thermal conductivity, and heat capacity）, geometry (film thickness and strip width）, and measurement parameters（frequency and intensity of the driving current）. Since the strips are larger than the film thickness, we find that the nanodot multilayers add frequency-independent offsets in the temperature rise with respect to the reference sample. We deduced the thermal resistance of the multilayer by performing measurements at the same heating power for all samples and by taking into account fluctuations in the strip widths and other relevant parameters. Error propagation in the used model equation is carried out through Monte Carlo simulation. More details can be found in the Supplementary material.

Atomistic Green's function calculation

This technique is discussed in Refs. [37-39]. A 1.63 · 1.63 nm^2 cross section of material comprising 72 atoms, with periodic boundary conditions in the x and y directions, is contacted on the z direction to two semi-infinite Si single crystals. Dispersion in the x and y directions is accounted for by a transverse wave-vector (k_x,k_y) grid, with a smallest step size of 0.03 nm^{-1}. Barriers are constructed by random substitution of Si by Ge atoms in regions 1 nm thick. Results were averaged over 50 different random configurations. The Tersoff interatomic potential for Si [40] is employed. Ge atoms are considered in the mass difference approximation. This is reasonable since most of the thermal resistivity is accounted for by mass difference [41]. Computational expense prevents us from treating larger cross sections. Therefore, the modulation due to the 20 nm diameter nanodots is included via a self-energy. A mean-field diagonal approximation to the retarded self-energy matrix is employed, with non-zero elements only associated to the atoms belonging to the barrier. We assumed an uncorrelated dot distribution. The dots are lens shaped, 20 nm in diameter, and 2 nm in height, with a $Si_{0.5}Ge_{0.5}$ composition. Local current conservation is imposed to compute the nonequilibrium Green's function and the phonon transmission through the system. The mean free paths are evaluated similarly as in Ref. [40]. Details will be given in a separate publication.

References

[1] Cahill, D. G. *et al.* Nanoscale thermal transport. *J. Appl. Phys.* **93,** 793-818 (2003).

[2] Shakouri, A. Nanoscale Thermal Transport and Microrefrigerators on a Chip. *Proceedings of IEEE* **94(8)**, 1613-1638 (2006).

[3] Chowdhury, I. *et al.* On-chip cooling by superlattice-based thin-film thermoelectrics. *Nature Nanotechnology* **4,** 235-238 (2008).

[4] Zeng, G. *et al.* Eras:InGaAs/InGaAlAs superlattice thin-film power generator array. *Appl. Phys. Lett.* **88**, 113502 (2006).

[5] Kim, W., Zide, J., Gossard, A., Klenov, D., Stemmer, S., Shakouri, A. & Majumdar, A. Thermal conductivity reduction and thermoelectric figure of merit increase by embedding nanoparticles in crystalline semiconductors. *Phys. Rev. Lett.* **96,** 045901 (2006).

[6] Lee, S. M., Cahill, D. G. & Venkatasubramanian, R. Thermal conductivity of Si-Ge superlattices. *Appl. Phys. Lett.* **70**, 2957-2959 (1997).

[7] Lee, M.L. & Ventkatasubramanian, R. Effect of nanodot areal density and period on thermal conductivity in SiGe/Si nanodot superlattices. *Appl. Phys. Lett.* **92,** 053112 (2008).

[8] Chiritescu, C. *et al.* Ultralow thermal conductivity in disordered, layered WSe_2 crystals. *Science* **315**, 351-353 (2007).

[9] Cahill, D. G., Watson, S. K. & Pohl, R. O. Lower limit to the thermal conductivity of disordered crystals. *Phys. Rev. B* **46,** 6131-6140 (1992).

[10] Swartz, E. T. & Pohl, R. O. Thermal boundary resistance. *Rev. Mod. Phys.* **61**, 605-668 (1989).

[11] Highland, M. *et al.* Ballistic-phonon heat conduction at the nanoscale as revealed by time-resolved x-ray diffraction and time-domain thermoreflectance. *Phys. Rev. B* **76**, 075337 (2007).

[12] Schmidt, O. G., Denker, U., Christiansen, S. & Ernst, F. Composition of self-assembled Ge/Si islands in single and multiple layers. *Appl. Phys. Lett.* **81**, 2614-2616 (2002).

[13] Liu J.L. *et al.* Cross-plane thermal conductivity of self-assembled Ge quantum dot superlattices. *Phys. Rev. B* **67,** 165333 (2003).

[14] Bao Y. *et al.* Electrical and thermal conductivity of Ge/Si quantum dot superlattices. *J. Electrochem. Soc.* **152,** G432-G435 (2005).

[15] Alvarez-Quintana J. *et al.* Cross-plane thermal conductivity reduction of vertically uncorrelated Ge/Si quantum dot superlattices. *Appl. Phys. Lett.* **93,** 013112 (2008).

[16] Dilhaire S., Rampnoux J. M., Claeys W., & Rossignol C., Optical heterodyne sampling device. Patent WO/2007/045773, 2006.

[17] Liu, X. *et al.* High thermal conductivity of a hydrogenated amorphous silicon film. *Phys. Rev. Lett.* **102**, 035901 (2009).

[18] Ezzahri, Y. *et al.* Coherent phonons in Si/SiGe superlattices. *Phys. Rev. B* **75,** 195309 (2007).

[19] Stevens, R. J., Smith, A. N., & Norris, P. M. Signal analysis and characterization of experimental setup for the transient thermoreflectance technique. *Rev. Sci. Instrum.* **77**, 084901 (2006).

[20] Huxtable, S. *et al.* Thermal conductivity imaging at micrometre-scale resolution for combinatorial studies of materials. *Nat. Mater.* **3**, 298-301 (2004).

[21] Cahill, D. G. Analysis of heat flow in layered structures for time-domain thermoreflectance. *Rev. Sci. Instrum.* **75**, 5119-5122 (2004).

[22] Schmidt, A. J., Chen, X., & Chen, G. Pulse accumulation, radial heat conduction, and anisotropic thermal conductivity in pump-probe transient thermoreflectance. Rev. Sci. Instrum. **79**, 114902 (2008).

[23] Ezzahri, Y. *et al.* Cross-plan Si/SiGe superlattice acoustic and thermal properties measurement by picosecond ultrasonics. *J. Appl. Phys.* **101**, 013705 (2007).

[24] Antonelli, G. A., Perrin, B., Daly, B. C., & Cahill, D. G. Characterization of mechanical and thermal properties using ultrafast optical metrology. *MRS Bull.* **31,** 607-613 (2006).

[25] Koh, Y. K., Singer, S. L., Kim, W., Zide, J. M. O., Lu, H., Cahill, D. G., Majumdar, A., & Gossard, A. C. Comparison of the 3 omega method and time-domain thermoreflectance for measurements of the cross-plane thermal conductivity of epitaxial semiconductors. *J. Appl. Phys.* **105,** 054303 (2009).

[26] Mingo, N. Calculation of si nanowire thermal conductivity using complete phonon dispersion relations. *Phys. Rev. B* **68**, 113308 (2003).

[27] Cahill D.G., Katiyar M. & Abelson J.R., Thermal conductivity of *a*-Si:H thin films. *Phys. Rev. B.* **50,** 6077-6081 (1994).

[28] Boukai, A. *et al.* Silicon nanowires as efficient thermoelectric materials. *Nature* **451,** 168-171 (2008).

[29] Vining, C. B. Desperately seeking silicon. *Nature* **451,** 132-133 (2008).

[30] Hochbaum, A. I. *et al.* Enhanced thermoelectric performance of rough silicon nanowires. *Nature* **451,** 163-167 (2008).

[31] Simkin, M. V. & Mahan, G. D. Minimum thermal conductivity of superlattices. *Phys. Rev. Lett.* **84**, 927-930 (2000).

[32] Venkatasubramanian, R. Lattice thermal conductivity reduction and phonon localizationlike behavior in superlattice structures. *Phys. Rev. B* **61,** 3091-3097 (2000).

[33] Kleint, C. A., Chakraborty, S., Heinrich, A., Schneider, C. M., Schumann, J., Falke, M., & Teichert, S. Thermal conductivity in strain symmetrized Si/Ge superlattices on Si(111). *Appl. Phys. Lett.* **83,** 4184-4186 (2003).

[34] Abeles, B. Lattice thermal conductivity of disordered semiconductor alloys at high temperatures. *Phys. Rev.* **131,** 1906-1911 (1963).

[35] Mingo, N. *et al.* Nanoparticle-in-alloy approach to efficient thermoelectrics: silicides in SiGe. *Nano Lett.* **9**, 711-715 (2009).

[36] Cahill D. G. & Pohl R. O., Thermal conductivity of amorphous solids above the plateau, *Phys. Rev. B* **35,** 4067-4073 (1987).

[37] Mingo, N. & Yang, L. Phonon transport in nanowires coated with an amorphous material: An atomistic green's function approach. *Phys. Rev. B* **68**, 245406 (2003).

[38] Zhang, W., Mingo, N., & Fisher, T. S. Simulation of phonon transport across a non-polar nanowire junction using an atomistic green's function method. *Phys. Rev. B* **76**, 195429 (2007).

[39] Savic, I., Mingo, N., & Stewart, D. A. Phonon transport in isotope-disordered carbon and boron-nitride nanotubes: Is localization observable? *Phys. Rev. Lett.* **101,** 165502 (2008).

[40] Tersoff, J. New empirical model for the structural properties of silicon. *Phys. Rev. Lett.* **56,** 632-635 (1986).

[41] Skye A. & Schelling P. K., Thermal resistivity of Si-Ge alloys by molecular-dynamics simulation. *J. Appl. Phys.* **103,** 113524 (2008).

[42] Chen, G., Thermal conductivity and ballistic-phonon transport in the cross-plane direction of superlattices, *Phys. Rev. B* **57,** 14958-14973 (1998).

Acknowledgments

This work was supported by the EU (Nano-thermoelectrics, IRG 39302), ANR (Thermaescape, ANR-06-NANO-054-01, Accatone), (EThNA, ANR-06-NANO-020), (OCTE, ANR-06-BLAN-129), the Conseil Régional d'Aquitaine (projet Photon et Phonons, 2007), the DFG (SPP1386, RA 1634/5-1), the European Regional Development Fund (n. 4212/09-13) and the State of Saxony. We acknowledge A. Hiess, Ch. Mickel, G. Scheider, T. Dienel, C.C. Bof Bufon, S. Harazim, D. Grimm, S. Baunack, and B. Eichler for experimental assistance, B. Rellinghaus for access to the Tecnai T20 TEM and A. Rotondi (Univ. Pavia) for insightful discussions on error propagation in the 3ω method measurements.

Author contributions

G. P. and J-M. R. performed the HPTR measurements and analysis; M. S., U. D., and O. G. S. grew the samples; G.S. and M.P. metalized the samples for HPTR. F. P. and M. S. performed AFM measurements; F. P., P. C., and A.R. performed the 3ω measurements and analysis, on a setup realized by A. J.; P. C., J. S., and I. M. processed and characterized the samples for 3ω measurements; C. D. performed the TEM measurements; I.S. carried out the Green's function calculation. I.S., S.W. and N.M. developed the theory. A.R., S.D., and N.M. coordinated the work and wrote the paper.

Additional information

The authors declare that they have no competing financial interests. Supplementary information accompanies this paper.

Figure captions

Figure 1: Sample structure. a) Sketch of the self-assembled nanodot multilayers fabricated by MBE. b) Bright field TEM image of a sample with t_{Si} = 12 nm. Dark areas correspond to the Ge layers. The inset shows a high-resolution TEM of a nanodot. c) AFM image of a single Ge/Si(001) dot layer prior to overgrowth with Si. d) AFM image of the topmost layer of a sample with t_{Si} = 3 nm.

Figure 2: Thermal response of the Ge nanodot multilayers. a) Experimental thermal resistance divided by the number of layers, for the 5 and 11 layer systems, measured by HPTR, and the 11 layer system measured by the 3ω technique, as a function of the average distance between layers, *L*. b) Experimental thermal conductivities corresponding to the systems in Fig. 2(a). The solid line is the result of the diffuse mismatch model. c) Thermal resistance per barrier, normalized by average amount of Ge in the barrier (given as an effective length), for the systems of Fig. 2(a). d) Thermal conductivities computed via Atomistic Green's Functions for 4 barriers. Diamonds: nanodot-barriers. Triangles: flat barriers. The experimental results from figure 2(b) are also shown for comparison.

Figure 3: Heterodyne picosend thermoreflectance set-up. Illustration of the optical bench in heterodyne configuration. Two femtosecond frequency-locked lasers operating in the near infrared, at two repetition rates close to 80MHz, are focused on the sample. A synchro photodiode is used to trigger the acquisition of the signal. The signal is acquired over 13ns with a sub-picosecond time resolution.

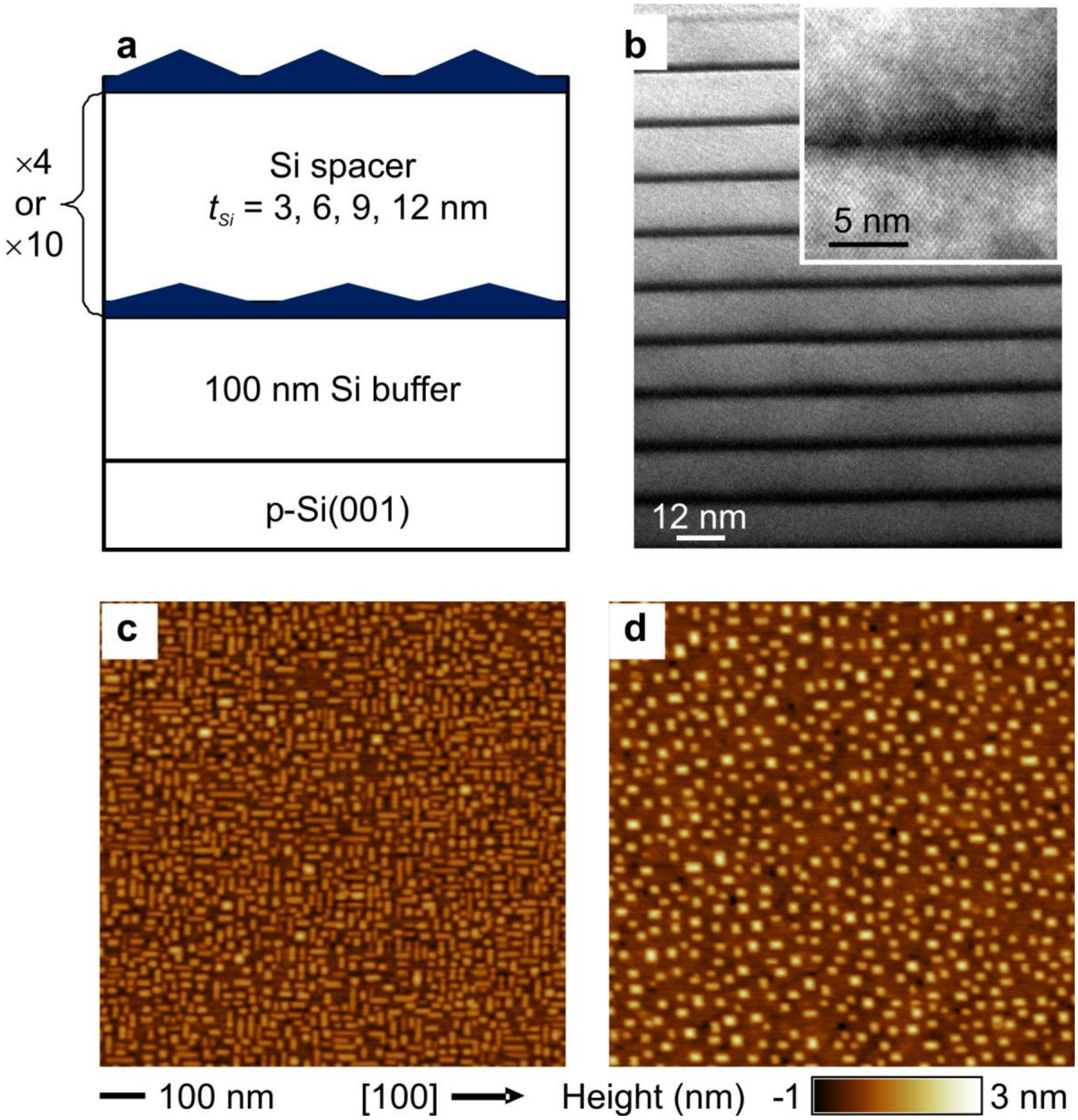
a
×4
or
×10
Si spacer
tSi = 3, 6, 9, 12 nm
100 nm Si buffer
p-Si(001)
b
5 nm
12 nm
c
d
100 nm
[100]
Height (nm)
-1
3 nm

FIGURE 1

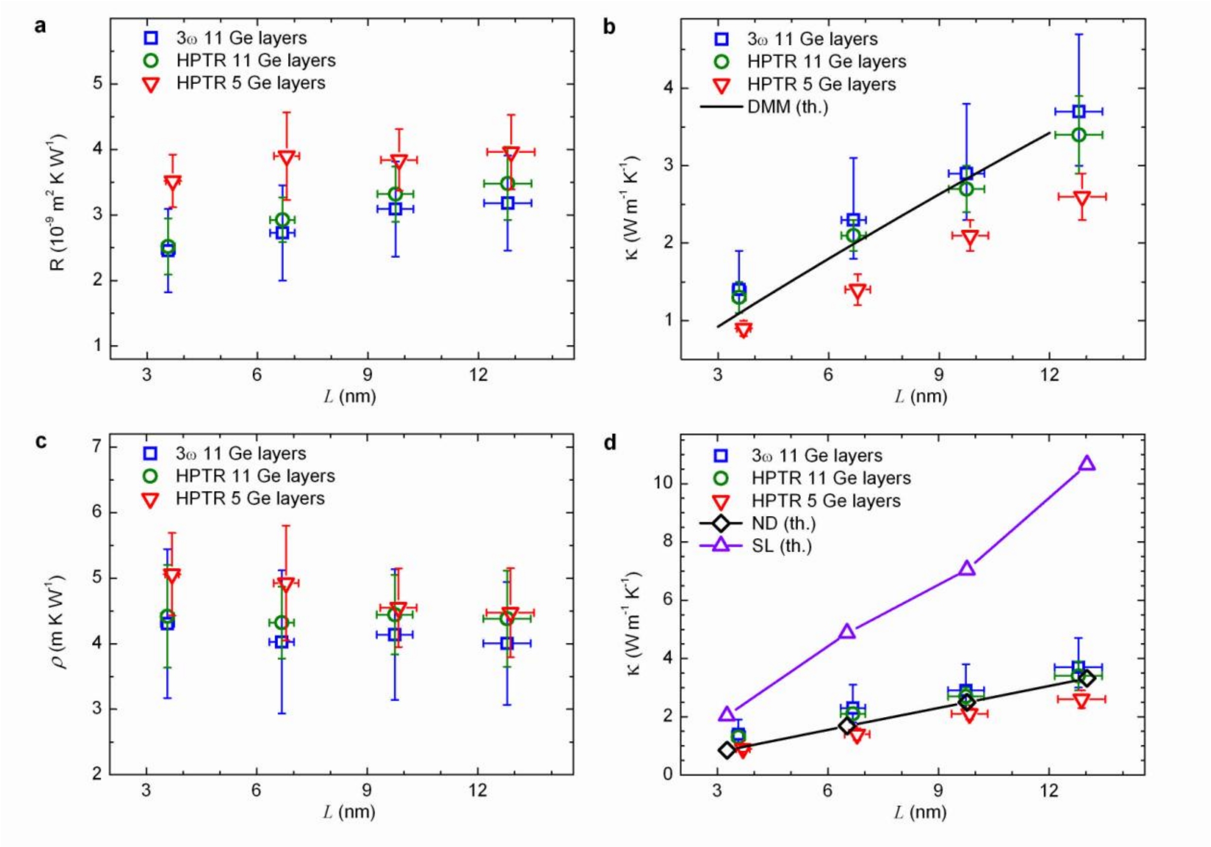
a
3ω 11 Ge layers
HPTR 11 Ge layers
HPTR 5 Ge layers
R (10^{-9} m^2 K W^{-1})
L (nm)
b
DMM (th.)
κ (W m^{-1} K^{-1})
c
ρ (m K W^{-1})
d
ND (th.)
SL (th.)

FIGURE 2

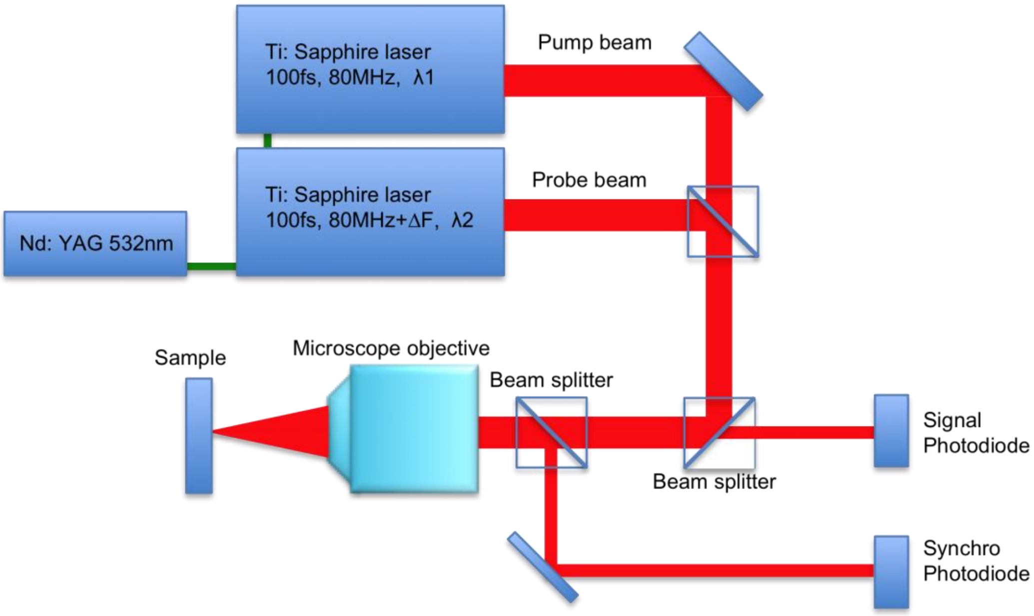
Ti: Sapphire laser
100fs, 80MHz, λ1
Pump beam
Ti: Sapphire laser
100fs, 80MHz+ΔF, λ2
Probe beam
Nd: YAG 532nm
Sample
Microscope objective
Beam splitter
Beam splitter
Signal
Photodiode
Synchro
Photodiode

FIGURE 3